




Mechanical and oxidation resistance of remanufactured NiCoCrAlYTa coating deposited via arc ion plating

Tao Fan^{1,2}, Jihua Peng^{1,*} , Qian Shi², Songsheng Lin², Mingjiang Dai², Peng Tang², Caifeng Zheng³, and Hongzhi Yang⁴

¹School of Material Science and Engineering, South China University of Technology, Guangzhou 510640, China

²Institute of New Materials, Guangdong Academy of Science, National Engineering Laboratory for Modern Materials Surface Engineering Technology, Key Lab of Guangdong for Modern Surface Engineering Technology, Guangzhou 510651, China

³China National South Aviation Industry Co, Ltd, Zhuzhou 412000, China

⁴Key Laboratory of Materials Design and Preparation Technology of Hunan Province, School of Materials Science and Engineering, Xiangtan University, Xiangtan 411105, China

Received: 27 June 2022

Accepted: 26 September 2022

Published online:

18 October 2022

© The Author(s), under exclusive licence to Springer Science+Business Media, LLC, part of Springer Nature 2022

ABSTRACT

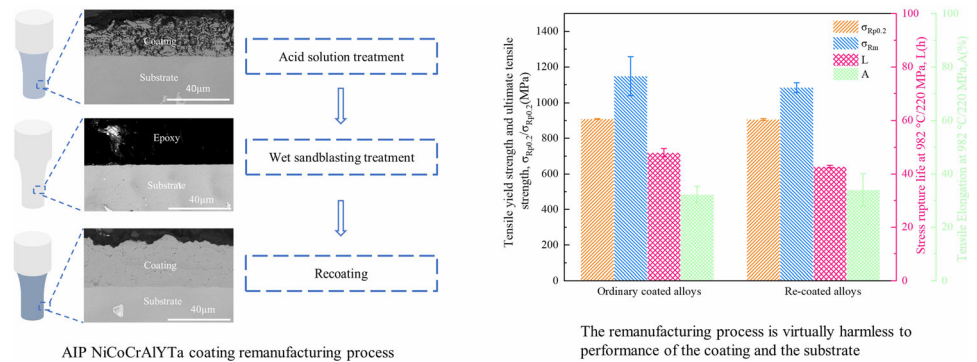
NiCoCrAlYTa coating of the Ni-based superalloy substrate was processed using a feasible remanufacturing method. The coating was deposited using arc ion plating (AIP) and removed by a complex treatment of immersion-etching in hydrochloric acid solution and wet sandblasting. The conventional and remanufactured coatings were homogenized in vacuum at 1080 °C for 4 h and then oxidized isothermally in the air at 1050 °C for 200 h. The constituent phases and the microstructure were characterized using powder X-ray diffraction (XRD) and field emission scanning electron microscopy (FE-SEM). Additionally, the mechanical performance of the coated specimens was evaluated via tensile testing at room temperature and stress rupture testing at 982 °C/220 MPa. The complex treatment is found to effectively remove the NiCoCrAlYTa coating without causing damage to the substrate. The re-coated specimens had a tensile yield strength greater than 985 MPa at room temperature, a rupture life of 45 h at 982/220 MPa, and an oxidation rate constant K_p of $3.16 \times 10^{-12} \text{ g}^2\text{cm}^{-4} \text{ s}^{-1}$ at 1050 °C, which were nearly identical to those of the conventionally coated specimens.

Handling Editor: Maude Jimenez.

Address correspondence to E-mail: jhpeng@scut.edu.cn

<https://doi.org/10.1007/s10853-022-07786-5>

GRAPHICAL ABSTRACT



Introduction

Owing to their superior oxidation resistance at high temperatures, MCrAlY (M: Ni, Co, or Ni + Co) coatings have been widely used to protect Ni-based superalloy components from oxidation and corrosion in high-temperature environments [1–3]. The high-temperature oxidation resistance properties of MCrAlY coatings are derived from the outward diffusion of aluminum elements from coating to surface, resulting in the formation of a dense α -Al₂O₃ scale on the coating surface [4]. Consequently, it is important to pay close attention to manufacturing defects and coating failures during the production process. Moreover, to extend the service life of substrates, repairing the coating without degrading the substrate by removing the original failed coating and applying a new coating [5] is a cost-effective and practical approach.

Traditional coating removal techniques include sandblasting [6], polishing [7, 8], and high-pressure water injection [9]. However, the powerful impact forces generated by these techniques may alter the shape profile of the Ni-based superalloy components. Currently, the majority of high-temperature oxidation resistance coatings are removed using chemical methods [10]. Bouchaud et al., utilized cathodic polarization to promote oxide flaking via hydrogen bubbling [11] in electrolytes containing inorganic acids and organic solvents, including ethanol. In contrast to β -NiAl, the solubility and outward-

diffusion capacity of Cr in γ' -Ni₃Al increased, resulting in a large difference between the constituent phases of the top oxide scale of the oxidized aluminide-coatings from pure Ni and Ni20Cr substrates [12]. Consequently, the removal rate of the aluminide coatings was significantly slower for the latter substrates when using cyclical potential stripping [12]. The chemically prepared PtAl coatings on Ni-based superalloys were easily removed by a solution containing HCl, H₃PO₄, and H₂O [5]. Clearly, the removal of high-temperature protective coatings is contingent on their composition and the methods of preparation. MCrAlY coatings are an important thermal barrier for superalloy-based components, and the remanufacturing process must account for the removal efficiency of unqualified coatings. However, there are few reports concerning the removal efficacy of MCrAlY coatings deposited by arc ion plating (AIP), which can produce a denser and more uniform coating than the thermal spray method.

The mechanical properties of the substrate and the oxidation resistance of re-coated MCrAlY coatings must also be considered, as they are inevitably affected by the coating-removal procedure [8–11]. When re-coating the surface of IC6 alloy with NiCrAlYSi, the room-temperature mechanical properties of the substrates could be maintained while the stress-rupture life was decreased at 1100 °C/90 MPa [13]. Compared to conventional coatings, the oxide scale on re-coated NiCoCrAlY coating on Ni-based alloys was more susceptible to peeling [14]. The high-

temperature oxidation resistance of the re-coated coatings was responsible for the previous removal depth of the interdiffusion layer of the oxidized CoCrAlY coatings [15], which was removed using a physical stripping technique. This suggests that, during remanufacturing, the effect of the removal step on the performance of the repair coatings, such as mechanical properties and corrosion resistance, must be carefully evaluated.

In this study, NiCoCrAlYTa coatings were deposited using AIP onto DZ22B Ni-based superalloy substrates. Additionally, the effect of a removal method combining electrochemical stripping and sandblasting on the mechanical and oxidation-resistant performance of repaired coatings was studied. Accordingly, the findings of this study were found to be applicable to the remanufacturing of the thermal barrier of Ni-based alloys.

Experimental materials and methods

Substrate and coating preparation

Ingots of the Ni-based superalloy were cut into rectangle specimens measuring 30 mm × 10 mm × 1.2 mm for oxidation and microstructure tests and rod-shaped specimens measuring 33 mm in gauge length and 8 mm in diameter for mechanical property tests. Table 1 displays the nominal composition of the DZ22B substrate and the target for AIP coatings. Before deposition, the surface of the substrate was wet-sandblasted to improve adhesion, then cleaned with acetone and alcohol, and finally dried in a hot air oven for 30 min. Similar to our previous studies [16, 17], a NiCoCrAlYTa coating with a thickness of approximately 30–40 μm was deposited on the specimen surface by AIP, and the processing parameters for the deposition of the ordinary and secondary repair coatings are shown in Table 2. To homogenize the chemical components, the specimens were annealed for 4 h at 1080 °C in a vacuum furnace. For convenience, the standard NiCoCrAlYTa coating will

henceforth be referred to as O-C# and the re-coated NiCoCrAlYTa coating as R-C#.

Coating removal

To avoid maximum surface damage during the coating removal process, the NiCoCrAlYTa-coated specimens were etched for less than 10 min in a 10% hydrochloric acid solution at 70 °C in a Ni-based alloy substrate. Thereafter, they were wet-blasted with a 200-mesh alumina powder suspension in water for 20–60 min under a pressure of 2 atm.

Performance and microstructure characterization

The coated specimens were tested for tensile strength and elongation at room temperature using a CMT4204 material testing machine with a strain rate of $1 \times 10^{-3} \text{ s}^{-1}$. Life and fracture-elongation of stress rupture were measured at 982 °C under a constant tensile stress of 220 MPa. The isothermal oxidation test was conducted in air at 1050 °C for 200 h, and the weight gain was measured every 25 h using a 0.1 mg-resolution precision optical balance. To protect the oxide scale during the preparation of the metallographic coupons, a Ni-layer was applied to the oxidized specimens.

X-ray diffraction (XRD, Smartlab 9 kW, Cu K α) was used to determine the phases of the NiCoCrAlYTa coatings. Scanning electron microscopy (SEM, Nova NanoSEM 430) and energy dispersive spectroscopy (EDS) were utilized to examine the chemical

Table 2 Plating parameters for NiCoCrAlYTa coatings

Plating parameters	NiCoCrAlYTa coating
Arc current (A)	120
Substrate via voltage (V)	−110
Pressure (Pa)	1.2
Bias source duty cycle (%)	65
Bias source frequency (Hz)	40

Table 1 Nominal compositions of the cast alloy DZ22B and the NiCoCrAlYTa cathodes (wt.%)

Component	Ni	Co	Cr	Al	W	Ti	Nb	P	S	Y	Ta
DZ22B	Bal	9	8	5	8	1	0.85	0.001	0.0005	–	–
NiCoCrAlYTa	Bal	17	11	9	–	–	–	–	–	0.8	1.2

composition, surface morphologies, and fractography of the specimens.

Results and discussion

Microstructural evolution of the coatings during coating-removing-recoating

Figure 1a depicts the cross-sectional micromorphology of O-C#. It had a thickness of approximately 30 μm and was primarily composed of the γ -Ni phase, γ' -Ni₃Al phase, and a small amount of the β -NiAl phase. Typical NiCoCrAlYTa coatings undergo elemental diffusion between coating and substrate following vacuum heat treatment, resulting in the elimination of voids as depicted in Fig. 1b. Figure 1c depicts the X-ray diffraction spectrum of the O-C# coating before and after vacuum heat treatment. After vacuum heat treatment, the β -NiAl phase with (220) and (211) characteristic diffraction peaks gradually disappear, and the γ -Ni/ γ' -Ni₃Al phases with (111), (200), and (220) diffraction peaks become sharp [16].

Figure 2a depicts the cross-sectional morphologies of the original NiCoCrAlYTa coating following a 5-min etching. NiCoCrAlYTa coating thickness did not decrease significantly; however, the coating's interior had corroded and become loose. The top surface SEM image of the 5 min-etched specimens is depicted in Fig. 2b, which reveals that the surface became uneven and contained numerous voids. After 10 min of etching, as depicted in Fig. 2c and d, the coating became thinner but was not completely removed; some coating residue still protected the substrate from severe etching. Wet sandblasting was performed to completely remove the remaining coating and minimize the impact of hydrochloric acid

corrosion on the substrate. Figure 2e and f displays the cross section and top surface images of the specimens following 10 min of etching and 30 min of wet sandblasting.

During coating removal, Al, Cr, Ni, and Co have standard potentials of -1.66 , -0.74 , -0.25 , and -0.28 V, respectively [18–21]. Aluminum and chromium react violently with hydrochloric acid, whereas nickel and cobalt react slowly. These corresponding hydrogen-releasing reactions are depicted by Eqs. (1–4). These reactions promote the formation of voids or pinholes in the coatings, which is advantageous for the ingress of hydrochloric acid. Thus, the process of surface thinning and partial stripping can be accelerated.

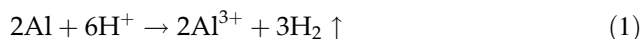


Figure 3a and b depicts the cross-sectional images of R-C# coatings before and after vacuum heat treatment, respectively. Similar to the O-C# coatings, the elimination of voids in the coatings was caused by elemental diffusion during vacuum heat treatment. In addition to the blurring of the coating-substrate boundary, no defects are visible in Fig. 3b. Figure 3c displays the X-ray diffraction spectrum of the R-C# coatings. There is no distinction between O-C# and R-C# specimens in terms of microstructure and phase composition. Overall, the effect of the complex removal treatment in this study on the R-C# microstructure can be disregarded.

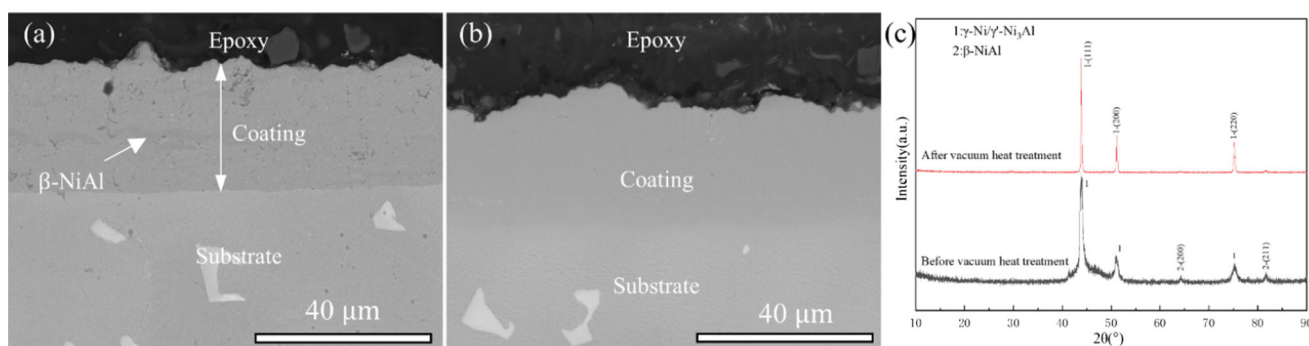


Figure 1 SEM cross-sectional image of O-C# (a/b) and its XRD patterns (c) before and after vacuum heat treatment.

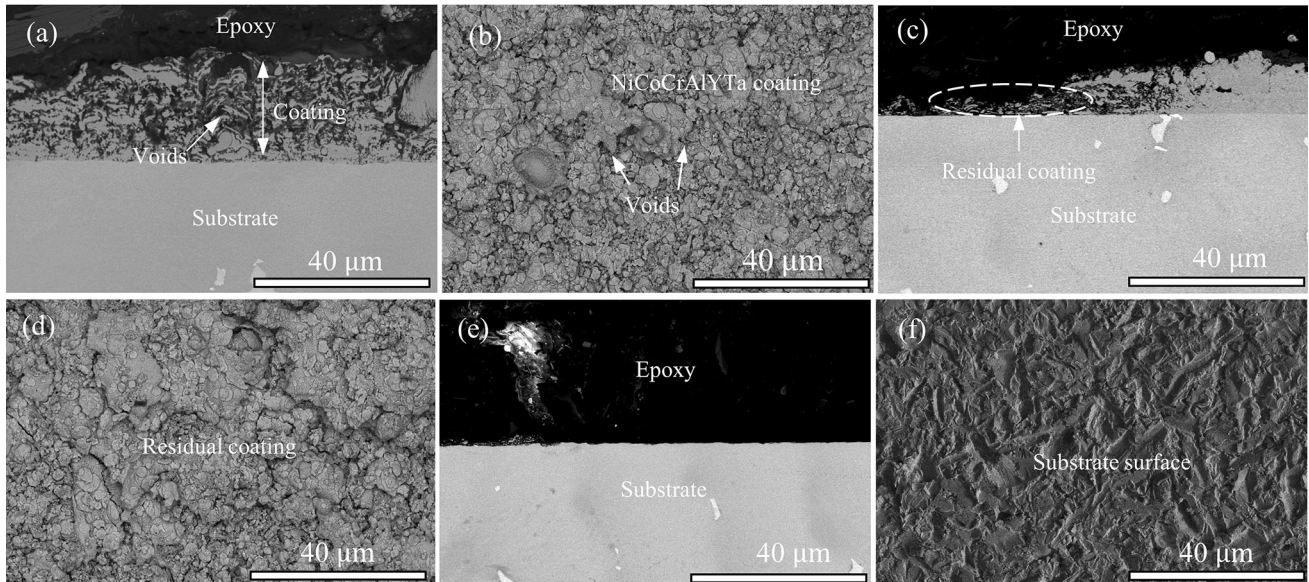


Figure 2 Cross-sectional and surface images after etching for 5 min (a, b), after etching for 10 min (c, d), and after wet blasting (e, f).

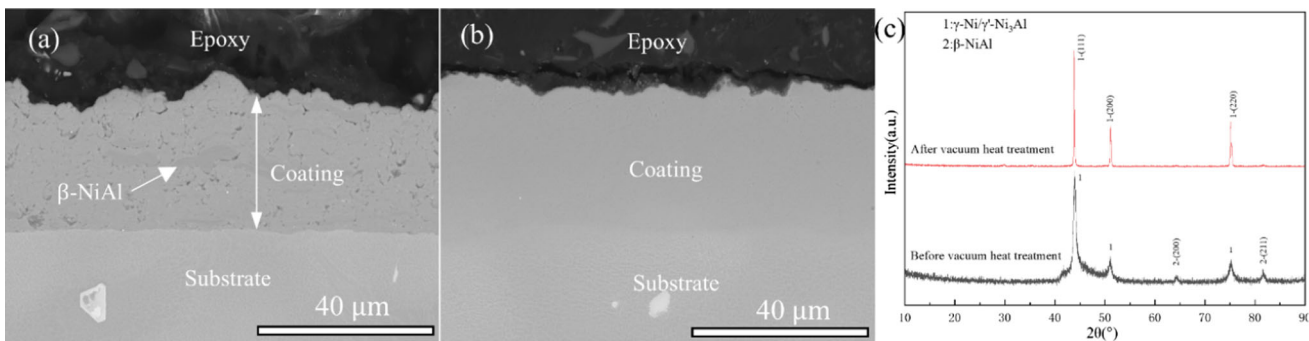


Figure 3 SEM cross-sectional image of R-C# (a/b) and its XRD patterns (c) before and after vacuum heat treatment.

Mechanical properties

Tensile testing

It is necessary to investigate the effect of substrate removal and reapplication on its mechanical properties. Neither O-C#- nor R-C#-coated specimens exhibited necking during room-temperature tensile tests in air, exhibiting the typical brittle fracture. Figure 4 depicts the tensile fractographic images of O-C# and R-C# specimens at room temperature. The macroscopic fracture morphology appeared comparable to that depicted in Fig. 4a, c. In the high-resolution images (Fig. 4b and d), the fracture surfaces exhibit a lamellar structure with numerous secondary cracks. Some smooth terraces were formed in the W-rich precipitated phase depicted in Fig. 4f (Spot 2), and numerous tear edges were observed in the γ/γ'

phase zone of the substrate. The EDS chemical compositions of Spot 1 and Spot 2 are also attached. There are no internal fractures and voids at the coating-substrate interface after fracture, indicating a strong adhesion.

The tensile results at room temperature are depicted in Fig. 5, where σ_{Rm} represents the ultimate tensile strength, $\sigma_{Rp0.2}$ represents the yield strength, and A represents the tensile fracture-elongation. The ultimate strength and yield strength of the coated specimens were almost identical to those of the DZ22B alloy substrate, while the fracture-elongation was slightly reduced. Either R-C# or O-C# specimens were homogenized once at 1080 °C for 4 h under vacuum. The reduction of the average elongation of R-C# specimens was likely the cause of performance scattering due to the non-uniformity of microstructure in the substrates [22–24], because the

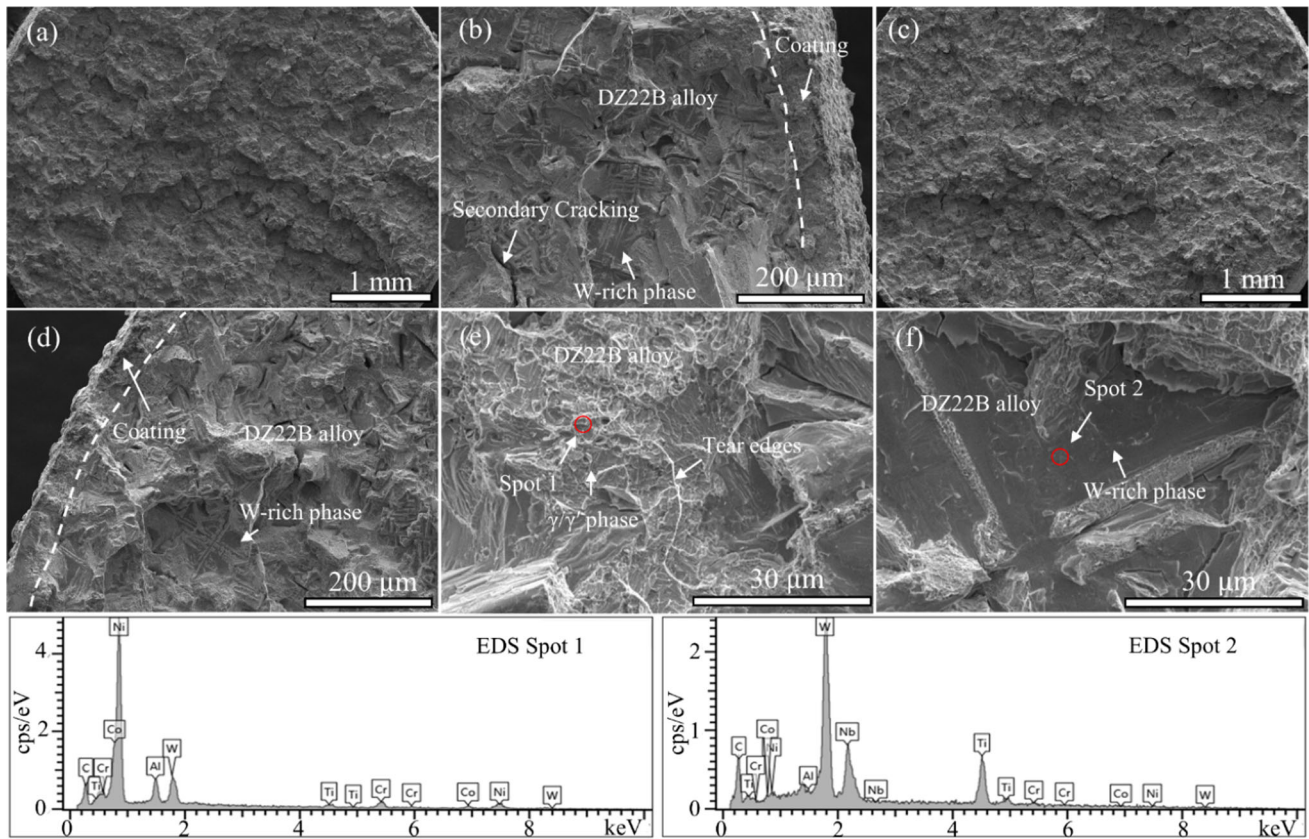


Figure 4 Room temperature tensile Fractographies of O-C#-coated (a, b) and R-C#-coated (c, d, e, f) specimens.

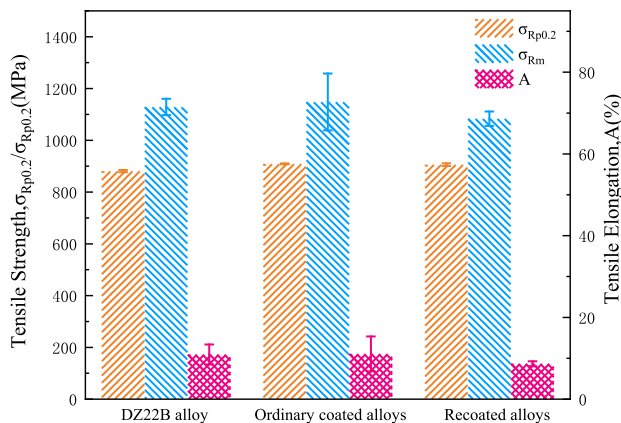


Figure 5 Room temperature tensile properties of DZ22B alloy and the coated specimens.

homogenization produced a small difference in the elemental composition of γ/γ' and precipitated phases. $\sigma_{Rp0.2}$ of the R-C# specimens was greater than 985 MPa, which is within the application requirement's tolerance range. Thus, the current study demonstrated that the effect of the remanufacturing process on tensile performance can be acceptable.

Stress rupture testing

The rupture life and rupture elongation of DZ22B alloy and NiCoCrAlYTa-coated specimens at 982 °C/220 MPa are depicted in Fig. 6. The NiCoCrAlYTa coating increases the rupture life by more than 20% in comparison to the DZ22B alloy. The average rupture

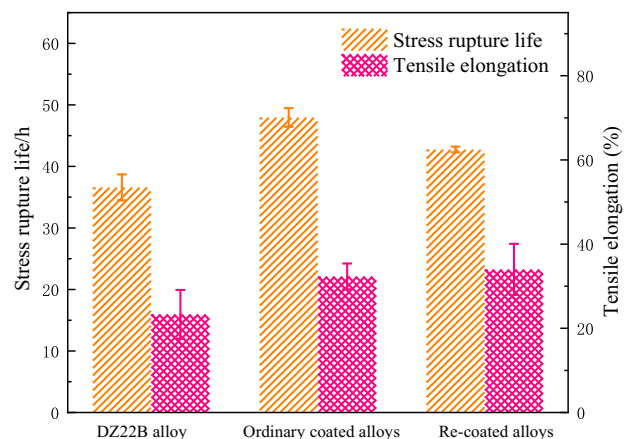


Figure 6 Tensile rupture performance of DZ22B alloy and the coated specimens under 982 °C/220 MPa.

elongation of R-C#-coated specimens was identical to that of O-C#-coated specimens, whereas its stress-rupture life was slightly diminished. However, the average strain rate remained approximately $0.6\% \text{ h}^{-1}$ for all specimens, exhibiting slight fluctuations.

The fracture surface morphologies of DZ22B alloy and O-C#- and R-C#-coated specimens at $982^\circ\text{C}/220 \text{ MPa}$ are illustrated in Fig. 7. In contrast to the fracture mode of the room-temperature tensile test depicted in Fig. 4, the fracture mode of the stress rupture specimens appears to be a typical mode of micro-void coalescence, as depicted in Fig. 7a2, b2, and c2. Figure 7a3 depicts a thick oxide layer on the fracture surface of a DZ22B alloy specimen. As depicted in Fig. 7a1, b1, and c1, the fractured surface of the DZ22B specimen exhibited significantly more cracks perpendicular to the force axis and larger voids than the fractured surface of the coated specimen. On the R-C# specimens, the parallel deformation lines to the force axis can still be seen. As shown in Fig. 7b3 and c3, the oxidation of the coating-substrate interface is significantly attenuated, despite the

presence of some cracks in the coatings. During this high-temperature, the short-duration rupture test, fracture behavior is still governed by the substrate via crack initiation and propagation via voids. The adhesion of the NiCoCrAlYTa coating to the substrate impeded the formation and growth of voids in the substrate, thereby enhancing the rupture life and rupture elongation.

Because the yield strength of the substrate at 982°C is greater than 200 MPa [22], the creep is caused by rupture elongation. The embrittled oxide layer on the DZ22B alloy prefers to become the crack initiation site. The stress concentration at the crack tip facilitates the formation of voids. Above 650 and 700°C , the ductile–brittle transition transformation of β – γ – γ' in MCrAlY coating occurs [23, 24], and the yield and tensile ultimate strengths of the NiCoCrAlYTa coatings at 850°C are only 58 and 65 MPa , respectively [25], so the formation of through-thickness cracks in the coatings is inevitable under $982^\circ\text{C}/220 \text{ MPa}$; however, their propagation stops near the interface (Fig. 7b3, c3). These coating fragments

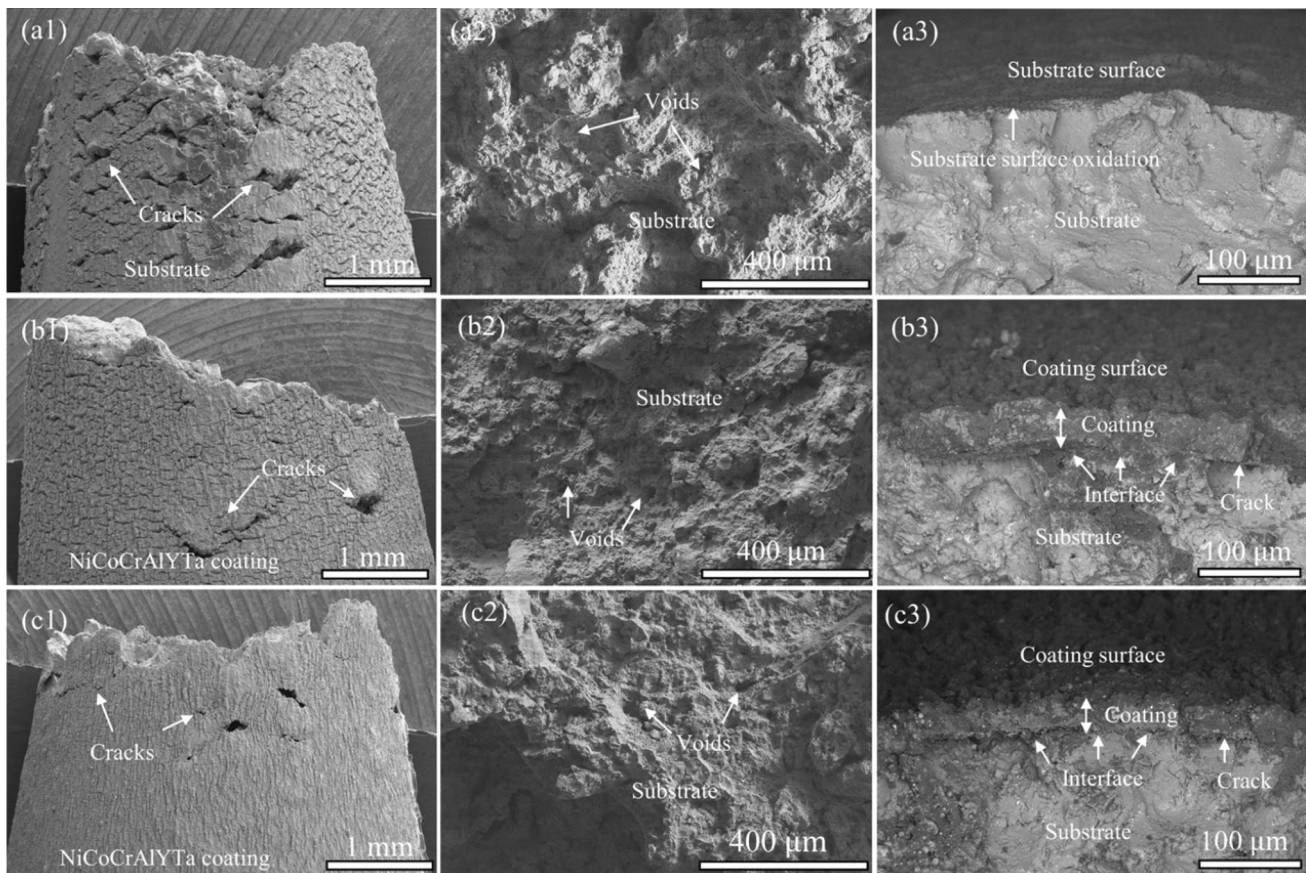


Figure 7 Fractography of the DZ22B (a1, a2, a3), O-C# (b1, b2, b3), and R-C#-coated (c1, c2, c3) specimens after rupture tests.

adhere strongly to the substrate and continue to protect it from oxidation.

The coating-removal step causes the accumulation of internal stresses and surface defects on the substrate and weakens the adhesion between the coating and substrate interface [26, 27]. Consequently, the effective load transferred to the coating of the R-C# specimen decreased, and the deformation lines in Fig. 7a1 can be maintained. Owing to the difference in elastic modulus between the coating and substrate, shear stress can be induced in the interface zone, leading to the formation of a de-adhesive crack parallel to the loading direction (Fig. 7b3, c3) and an increase in the thermal exposure area of the substrate. This fracture is larger in the R-C#-coated specimen than in the O-C#-coated specimen. Similar to other reports [28–31], these exposed interface regions can exacerbate the surface deterioration and coarsening of γ' -Ni₃Al precipitates on the substrates. Overall, the process of repairing the NiCoCrAlYTa coating has no negative effect on the high-temperature durability of the substrate, and the re-coated NiCoCrAlYTa coating can still improve the ductility of the substrate at 982 °C.

Oxidation resistance

Figure 8 depicts the oxidation kinetic curves of DZ22B alloy, O-C#-coated specimens, and R-C#-coated specimens at 1050 °C. The oxidation kinetic curve of DZ22B alloy (substrate) approximates a linear law, indicating that at 1050 °C, DZ22B alloy has

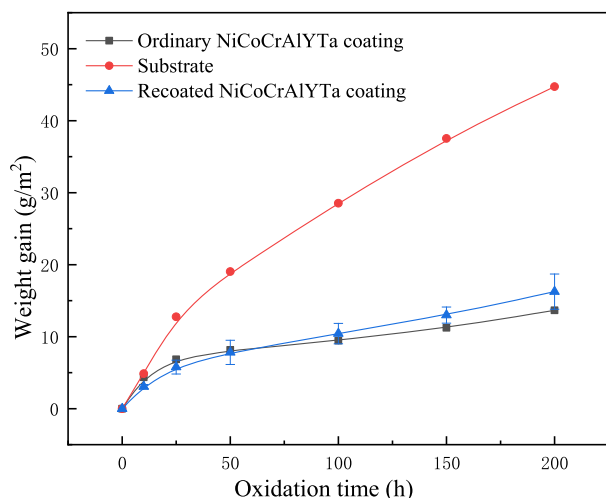


Figure 8 Isothermal oxidation kinetics of DZ22B alloy and the coated specimens at 1050 °C in air.

almost no oxidation resistance. Both O-C#-coated and R-C#-coated specimens initially undergo a rapid oxidation stage within the first 25 h, accompanied by a significant increase in weight; this is followed by a stable oxidation stage, which is typically dominated by the growth of the alumina scale [32, 33]. The oxidation kinetics curves of the two coated specimens roughly correspond to the parabolic oxidation kinetics law. O-C#- and R-C#-coated specimens have oxidation rate constants (K_p) of 2.59×10^{-12} and $3.16 \times 10^{-12} \text{ g}^2\text{cm}^{-4} \text{ s}^{-1}$, respectively. In previous studies, the oxidation constant for α -Al₂O₃ layer growth at 1000 °C was determined to be $10^{-14} \text{ g}^2\text{cm}^{-4} \text{ s}^{-1}$ [14, 34], indicating the presence of elements other than aluminum diffusing to the coating surface to participate in the reaction during isothermal oxidation of R-C#.

Figure 9 depicts the XRD patterns of a re-coated NiCoCrAlYTa coating that has been oxidized in air at 1050 °C for varying times. During the isothermal oxidation of R-C#, a series of oxides, including α -Al₂O₃, NiO, Cr₂O₃, and NiCr₂O₄, were produced as the reaction products of solute atoms with oxygen [35, 36]. The possible reaction processes of these oxides are listed in Eqs. (5–9) [37, 38]. Increasing the isothermal oxidation time weakens the oxide peaks of NiO, Cr₂O₃, and NiCr₂O₄, particularly the (111), (200), and (220) peaks of NiO, which gradually broaden and vanish. However, the characteristic (012), (104), and (116) peaks of α -Al₂O₃ intensify as oxidation progresses, indicating that the alumina-rich

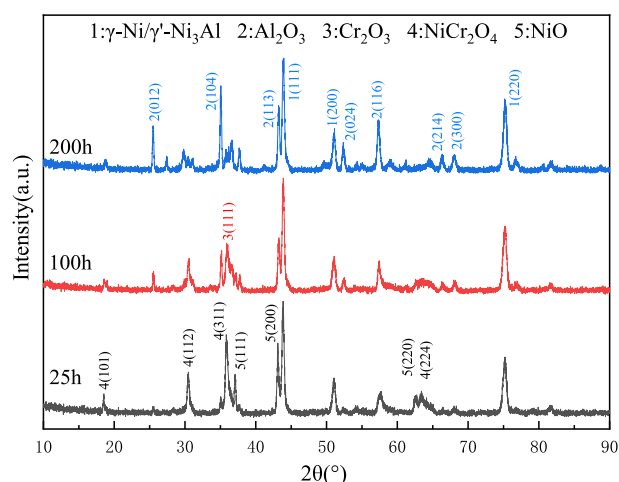
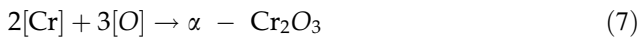
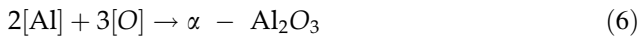


Figure 9 XRD patterns of the NiCoCrAlYTa re-coated specimens after oxidation at 1050 °C.

scale provides the greatest oxidation resistance [16, 39].



The cross-sectional morphologies of the re-coated NiCoCrAlYTa coatings after oxidation at 1050 °C for various times are depicted in Fig. 10. In Fig. 10a, after 25 h of oxidation, a thin but continuous almost pure α -Al₂O₃ scale (dark contrast arrow) is formed on the coating surface; and the mixed oxides (light contrast arrow) are sporadically distributed on top of this α -Al₂O₃ scale, which are responsible for many of the characteristic peaks shown in Fig. 9. Comparing the thickness of the pure Al₂O₃ scale of the 25 h oxidized specimen to that of the 100 h oxidized specimen, the pure Al₂O₃ scale of the 100 h oxidized specimen became thinner; the mixed-oxide layer became twice as thick, and the Al₂O₃ fraction in it increased; some voids formed locally in the mixed-oxide cluster zone, as indicated by the arrow in Fig. 10b. These voids within the oxide layer are likely the result of the Kirkendall effect caused by the diffusion of elements between the NiCoCrAlYTa coating and the oxide layer [40, 41], as well as the volume shrinkage

resulting from the transformation of θ -Al₂O₃ to α -Al₂O₃ [42–44]. After 200 h of oxidation (Fig. 10c), the oxide layer clearly separated into two sub-layers, one with a high fraction of Al₂O₃ (darker contrast) and one with a low fraction of Al₂O₃ (lighter contrast). EDS analysis reveals that Ni, Co, and Cr elements diffuse outward from the top surface, and large voids and cracks form in the sub-layer, resulting in the peeling off of the coating.

A continuous and dense scale of nearly pure α -Al₂O₃ contributes significantly to the oxidation resistance of MCrAlY-coated components by inhibiting the out-diffusion of various alloying elements. As oxidation progresses, voids and microcracks form in this pure α -Al₂O₃ sub-layer, leading to its fracture; subsequently, the oxidation of the NiCoCrAlYTa coating is exacerbated [45]. The solid-state reaction between the mixed oxides produces NiCr₂O₄ spinel, which influences the density of the mixed oxide [46–48]. In addition, voids and microcracks can be produced in the oxide layer by both oxide growth stresses and thermal expansion stresses [49, 50]. Because the affinity of Al with O is the strongest of all alloying elements, inward-diffusion O prefers to form α -Al₂O₃ to produce a dense growing sub-layer, while other elements tend to diffuse through this sub-layer to form a mixed-oxide top sub-layer. As shown in Fig. 1b, after the α -Al₂O₃ sub-layer is fractured, Al diffusion to the top surface accelerates, resulting in the formation of a mixed-oxide layer containing a

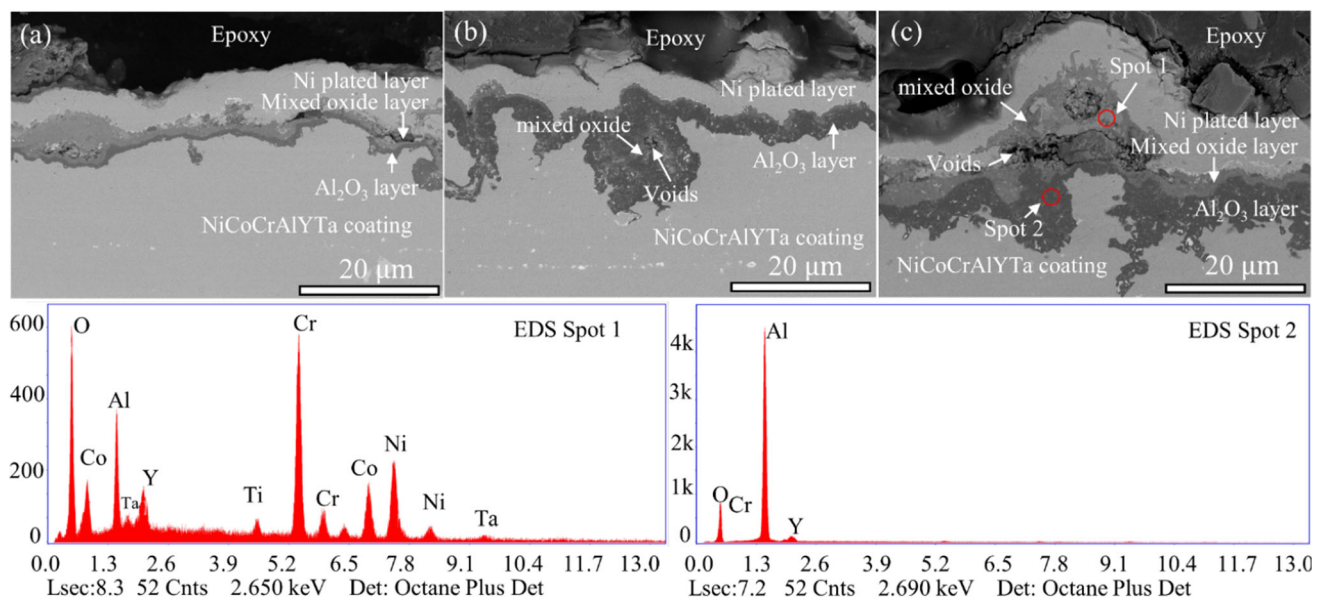


Figure 10 Cross-sectional images of the R-C# coating after oxidization for **a** 25 h, **b** 100 h, and **c** 200 h.

high proportion of Al_2O_3 compounds. Because the diffusion rate of Cr is slower than that of Al and Ni [12], particularly the high affinity with O fixes the Al in the bottom sub-layer of the oxide layer, as shown in Fig. 10c, a new top sub-layer with a low fraction of Al_2O_3 forms. The difference in K_p between R-C#- and O-C#-coated specimens is likely attributable to the defect density in the coating and interface during the removal step. This merits further study.

Conclusions

- (1) The deposited NiCoCrAlYTa coating can be removed completely and efficiently by a combining hydrochloric acid solution etching and wet sandblasting. The re-coated coating had the same constituent phases as the original coating after undergoing this complex removal procedure. Additionally, the re-coated DZ22B alloy specimens had a tensile yield strength of > 985 MPa at room temperature.
- (2) The conventional- and repair-NiCoCrAlYTa-coating-coated specimens exhibited greater stress-rupture life and fracture-elongation than the substrate alloy at $982\text{ }^\circ\text{C}/220$ MPa. During rupture tests, the re-coated specimens demonstrated a similar average creep strain rate of $\sim 0.6\% \text{ h}^{-1}$, which was similar to the DZ22B alloy-coated specimens and the conventional-coated specimens. The elimination step decreased the rupture life and elongation by a small amount.
- (3) When oxidized in air at $1050\text{ }^\circ\text{C}$, the oxidation kinetic curve of the specimens that were re-coated with NiCoCrAlYTa coating conformed to the parabolic oxidation law, similar to the conventional-coated specimens. The oxidation rate constant (K_p) for the standard coating- and repair coating-coated specimens was 2.59×10^{-12} and $3.16 \times 10^{-12} \text{ g}^2\text{cm}^{-4} \text{ s}^{-1}$, respectively.

Acknowledgements

This work was supported by Guangdong Special Support Program (No. 2019BT02C629), Science and Technology Program of Guangzhou (No. 202007020008), Science and Technology Program of

Guangdong (2020B1212060049), GDAS' Project of Science and Technology Development (2022GDASZH-2022010103), and the Scientific Research Fund of Guangdong Province (No. 2016A030312015).

References

- [1] Goti R, Betaille-Francoual M, Hourcastagne E, Viguier B, Crabos F (2014) Isothermal oxidation behaviour of NiCoCrAlYTa coatings produced by HVOF spraying and tribomet (TM) process. *Oxid Met* 81(1–2):105–113
- [2] Toscano J, Gil A, Huttel T, Wessel E, Naumenko D, Singheiser L, Quadackers WJ (2007) Temperature dependence of phase relationships in different types of MCrAlY-coatings. *Surf Coat Technol* 202(4–7):603–607
- [3] Meng G-H, Liu H, Liu M-J, Xu T, Yang G-J, Li C-X, Li C-J (2019) Highly oxidation resistant MCrAlY bond coats prepared by heat treatment under low oxygen content. *Surf Coat Technol* 368:192–201
- [4] Meng GH, Liu H, Liu MJ, Xu T, Yang GJ, Li CX, Li CJ (2020) Large-grain $\alpha\text{-Al}_2\text{O}_3$ enabling ultra-high oxidation-resistant MCrAlY bond coats by surface pre-agglomeration treatment. *Corros Sci* 163:13
- [5] Alam MZ, Sarkar SB, Das DK (2018) Refurbishment of thermally degraded diffusion Pt-aluminide (PtAl) bond coat on a Ni-base superalloy. *Surf Coat Technol* 354:101–111
- [6] Shipway PH, Bromley JPD, Weston DP (2007) Removal of coatings from polymer substrates by solid particle blasting to enhance reuse or recycling. *Wear* 263(1):309–317
- [7] Folkes J (2009) Waterjet—an innovative tool for manufacturing. *J Mater Process Technol* 209(20):6181–6189
- [8] Kompella S, Moylan SP, Chandrasekar S (2001) Mechanical properties of thin surface layers affected by material removal processes. *Surf Coat Technol* 146–147:384–390
- [9] Teimourian H, Shabgard MR, Momber AW (2010) De-painting with high-speed water jets: paint removal process and substrate surface roughness. *Prog Org Coat* 69(4):455–462
- [10] Yang X, Zhang J, Lu Z, Park HY, Jung YG, Park H, Koo DD, Sinatra R, Zhang J (2020) Removal and repair techniques for thermal barrier coatings: a review. *Trans Inst Met Finish* 98(3):121–128
- [11] Bouchaud B, Creus J, Rebere C, Balmain J, Pedraza F (2008) Controlled stripping of aluminide coatings on nickel superalloys through electrolytic techniques. *J Appl Electrochem* 38(6):817–825
- [12] Le Guevel Y, Grégoire B, Bouchaud B, Bihé P, Pasquet A, Thiercelin M, Pedraza F (2016) Influence of the oxide scale

- features on the electrochemical descaling and stripping of aluminide coatings. *Surf Coat Technol* 292:1–10
- [13] Song JX, Han YF, Li SS, Xiao CB (2005) Repair of NiCrAlYSi overlay coating on Ni₃Al base alloy IC6. *Intermetallics* 13(3):351–355
- [14] Wang J, Ji H, Chen M, Bao Z, Zhu S, Wang F (2020) High temperature oxidation and interdiffusion behavior of recoated NiCoCrAlY coating on a nickel-based superalloy. *Corros Sci* 175:108894
- [15] Lei Q, Hui P, Hongbo G, Shengkai G, Huibin X (2013) Interdiffusion behavior of recoated CoCrAlY coating/ DZ125 directionally solidified superalloy. *Acta Metall* 49(02):229–235
- [16] Yang HZ, Zou JP, Shi Q, Dai MJ, Lin SS, Du W, Lv L (2019) Analysis of the microstructural evolution and interface diffusion behavior of NiCoCrAlYTaN coating in high temperature oxidation. *Corros Sci* 153:162–169
- [17] Yang H Z, Zou J P, Shi Q, Wang D, Dai M J, Lin S S, Chen X X, Wang W, Xia XP (2020) Comprehensive study on the microstructure evolution and oxidation resistance performance of NiCoCrAlYTaN coating during isothermal oxidation at High temperature. *Corrosion Sci*, 175.
- [18] Harrington SP, Devine TM (2009) Relation between the semiconducting properties of a passive film and reduction reaction rates. *J Electrochem Soc* 156(4):C154–C159
- [19] Koura N, Nagase H, Sato A, Kumakura S, Takeuchi K, Ui K, Tsuda T, Loong CK (2008) Electroless plating of aluminum from a room-temperature ionic liquid electrolyte. *J Electrochem Soc* 155(2):D155–D157
- [20] Szabo S, Bakos I (2010) Reference electrodes in metal corrosion. *Int J Corros*, 756950 (756920 pp.)–756950 (756920 pp.).
- [21] Xiang M, Xu Z, Wu Q, Wang Y, Yan Z (2022) Selective electrooxidation of primary amines over a Ni/Co metal-organic framework derived electrode enabling effective hydrogen production in the membrane-free electrolyzer. *J Power Sources* 535:231461
- [22] Ding B, Ren W, Zhong Y, Yuan X, Zheng T, Shen Z, Guo Y, Li Q, Peng J, Brnic J, Gao Y, Liaw PK (2022) Revealing the influential mechanism of strain ranges on cyclic-life saturation during creep-fatigue in Nickel-based superalloy DZ445. *Int J Plast* 155:103320
- [23] Tao XP, Wang XG, Zhou YZ, Tan KJ, Liang JJ, Yang YH, Liu JL, Liu JD, Li JG, Sun XF (2020) Effect of Pt-Al bond-coat on the tensile deformation and fracture behaviors of a second-generation SX Ni-based superalloy at elevated temperatures. *Surf Coat Technol* 389:11
- [24] Jackson GA, Sun W, McCartney DG (2019) The influence of microstructure on the ductile to brittle transition and fracture behaviour of HVOF NiCoCrAlY coatings determined via small punch tensile testing. *Mater Sci Eng-Struct Mater Properties Microstruct Process* 754:479–490
- [25] Texier D, Monceau D, Crabos F, Andrieu E (2017) Tensile properties of a non-line-of-sight processed β - γ - γ' MCrAlY coating at high temperature. *Surf Coat Technol* 326:28–36
- [26] Wang H-Y, Zhu R-F, Lu Y-P, Xiao G-Y, He K, Yuan YF, Ma X-N, Li Y (2014) Effect of sandblasting intensity on microstructures and properties of pure titanium micro-arc oxidation coatings in an optimized composite technique. *Appl Surf Sci* 292:204–212
- [27] Li Z, Qian S, Wang W (2011) Influence of superalloy substrate roughness on adhesion and oxidation behavior of magnetron-sputtered NiCoCrAlY coatings. *Appl Surf Sci* 257(24):10414–10420
- [28] Bin Zaman S, Hazrati J, De Rooij M, Matthews D, Van Den Boogaard T (2021) Investigating AlSi coating fracture at high temperatures using acoustic emission sensors. *Surf Coat Technol* 423:13
- [29] Wang HW, Yang JX, Meng J, Ci SW, Yang YH, Sheng NC, Zhou YZ, Sun XF (2021) Effects of B content on microstructure and high-temperature stress rupture properties of a high chromium polycrystalline nickel-based superalloy. *J Alloy Compd* 860:11
- [30] Parlikar C, Alam MZ, Chatterjee D, Das DK (2019) Oxidation and concomitant effects on the microstructure and high temperature tensile properties of a DS Ni-base superalloy applied with different thicknesses of Pt-aluminide (PtAl) bond coat. *Surf Coat Technol* 373:25–37
- [31] Liu YD, Sun J, Li W, Gu WS, Pei ZL, Gong J, Sun C (2021) Microstructural evolution and mechanical properties of NiCrAlYSi plus NiAl/cBN abrasive coating coated superalloy during cyclic oxidation. *J Mater Sci Technol* 71:44–54
- [32] Wang J, Chen M, Cheng Y, Yang L, Bao Z, Liu L, Zhu S, Wang F (2017) Hot corrosion of arc ion plating NiCrAlY and sputtered nanocrystalline coatings on a nickel-based single-crystal superalloy. *Corros Sci* 123:27–39
- [33] Brandl W, Marginean G, Maghet D, Utu D (2004) Effects of specimen treatment and surface preparation on the isothermal oxidation behaviour of the HVOF-sprayed MCrAlY coatings. *Surf Coat Technol* 188:20–26
- [34] Brumm M W, Grabke HJ (1992) The oxidation behaviour of NiAl-I. Phase transformations in the alumina scale during oxidation of NiAl and NiAl-Cr alloys. *Corrosion Sci* 33(11):1677–1690.
- [35] Han YJ, Chen HF, Gao D, Yang G, Liu B, Chu YJ, Fan JK, Gao YF (2017) Microstructural Evolution of NiCoCrAlHfYSi and NiCoCrAlTaY Coatings Deposited by AC-HVAF and APS. *J Therm Spray Technol* 26(8):1758–1775

- [36] Puetz P, Huang X, Yang Q, Tang Z (2011) Transient oxide formation on APS NiCrAlY after oxidation heat treatment. *J Therm Spray Technol* 20(3):621–629
- [37] Zhu C, Li P, Wu XY (2016) A study of the diffusion and pre-oxidation treatment on the formation of Al₂O₃ ceramic scale on NiCrAlY bond-coat during initial oxidation process. *Ceram Int* 42(6):7708–7716
- [38] Cao F, Tryon B, Torbet CJ, Pollock TM (2009) Microstructural evolution and failure characteristics of a NiCoCrAlY bond coat in “hot spot” cyclic oxidation. *Acta Mater* 57(13):3885–3894
- [39] Rahman A, Jayaganthan R, Prakash S, Chawla V, Chandra R (2011) Cyclic high temperature oxidation behaviour of sputtered Cr/Al multilayer coatings on superalloy. *Surf Eng* 27(5):393–401
- [40] Audigé P, Rouaix-Vande Put A, Malié A, Bilhé P, Hamadi S, Monceau D (2014) Observation and modeling of α -NiPtAl and Kirkendall void formations during interdiffusion of a Pt coating with a γ -(Ni-13Al) alloy at high temperature. *Surf Coat Technol* 260:9–16
- [41] Zhou Y, Zhao X, Zhao C, Hao W, Wang X, Xiao P (2017) The oxidation performance for Zr-doped nickel aluminide coating by composite electrodepositing and pack cementation. *Corros Sci* 123:103–115
- [42] Tolpygo VK, Clarke DR (2000) Microstructural study of the theta-alpha transformation in alumina scales formed on nickel-aluminides. *Mater High Temp* 17(1):59–70
- [43] Peng X, Clarke DR, Wang F (2003) Transient-alumina transformations during the oxidation of magnetron-sputtered CoCrAl nanocrystalline coatings. *Oxid Met* 60(3–4):225–240
- [44] Huang Y, Peng X, Chen X-Q (2021) The mechanism of θ - to α -Al₂O₃ phase transformation. *J Alloy Compd* 863:158666
- [45] Poza P, Gómez-García J, Múnez CJ (2012) TEM analysis of the microstructure of thermal barrier coatings after isothermal oxidation. *Acta Mater* 60(20):7197–7206
- [46] Liu YZ, Zheng SJ, Zhu YL, Wei H, Ma XL (2016) Microstructural evolution at interfaces of thermal barrier coatings during isothermal oxidation. *J Eur Ceram Soc* 36(7):1765–1774
- [47] Mahesh RA, Jayaganthan R, Prakash S (2011) High temperature oxidation studies on HVOF sprayed NiCrAl coatings on superalloys. *Surf Eng* 27(5):332–339
- [48] Wang F, Geng S (2003) High temperature oxidation and corrosion resistant nanocrystalline coatings. *Surf Eng* 19(1):32–36
- [49] Tolpygo VK, Clarke DR (1999) Alumina scale failure resulting from stress relaxation. *Surf Coat Technol* 120–121:1–7
- [50] Liu P, Jiang P, Sun Y, Xu R, Wang T, Zhang W (2021) Numerical Analysis of stress evolution in thermal barrier coating system during two-stage growth of heterogeneous oxide. *Ceramics Int* 47(10, Part A):14311–14319.

Publisher's Note Springer Nature remains neutral with regard to jurisdictional claims in published maps and institutional affiliations.

Springer Nature or its licensor holds exclusive rights to this article under a publishing agreement with the author(s) or other rightsholder(s); author self-archiving of the accepted manuscript version of this article is solely governed by the terms of such publishing agreement and applicable law.